RATE-DEPENDENT OFF-AXIS COMPRESSIVE STRENGTH OF A UNIDIRECTIONAL CARBON/EPOXY LAMINATE AT HIGH TEMPERATURE

Masamichi KAWAI *, Satoru SAITO **, Jian-Qi ZHANG **,
Yi XIAO *, Hiroshi HATTA*****
*** Department of Engineering Mechanics and Energy, University of Tsukuba**
**** Graduate School of Systems and Information Engineering, University of Tsukuba**
***** ACTC, Institute of Aerospace Technology, JAXA**

Keywords: *unidirectional laminate, off-axis compression, tension-compression asymmetry, rate dependence, physically-based failure criterion, high temperature, CFRP*

Abstract

Off-axis compressive strength and its rate dependence of a unidirectional carbon/epoxy laminate are examined for various fiber orientations at high temperature. Static compression tests are carried out at two different strain rates for each fiber orientation. Fiber orientation dependence of off-axis compressive strength, associated failure modes, and the effect of strain rate are first elucidated. An asymmetry in strength between tension and compression is quantified by comparing the results of off-axis compression tests with those of off-axis tension tests at the same strain rates and test temperature. Then, a simple physically-based failure criterion that considers an influence of transverse compressive stress on the shear strength along fibers is tested for accuracy of prediction of the off-axis tensile and compressive strengths and the associated failure envelope at different strain rates. Finally, an extended viscoplasticity model for describing the rate-dependent nonlinear off-axis tensile and compressive deformation is developed, with an emphasis on description of the tension-compression asymmetry in viscoplastic deformation.

1. Introduction

The apparent ultimate compressive strength of unidirectional CFRP laminates when loaded in the fiber direction is generally much lower than the apparent ultimate tensile strength, and it often comes to a level as low as 50 percent of the tensile strength [1-3]. On the contrary, the transverse compressive strength turns about 40 percent higher than the transverse tensile strength [3, 4]. These experimental facts reveal that for the off-axis strength of unidirectional composite laminates is generally asymmetric in tension and compression, and a reference strength of unidirectional composite laminates for in-plane loading changes from compression to tension as the loading direction deviates from the fiber direction. For systematic quantification of ultimate strength of unidirectional composites, therefore, it is of great significance to evaluate the different off-axis strengths in tension and compression [5, 6].

Compressive failure of unidirectional composites is controlled by shear deformation and failure of the matrices for either on-axis or off-axis compressive loading. Shear deformation of polymer exhibits significant strain-rate dependence over a wide range of temperature. This fact further suggests that the compressive strength of unidirectional polymer matrix composites depends on the rate of compressive loading. To develop understanding of the compressive strength and controlling compressive failure mechanisms for unidirectional polymer matrix composites, therefore, not only the effect of stiffness and strength of the matrix but also the effect of relative orientation of the compressive load and the effect of rate-dependent deformation and strength of the matrix should appropriately be taken into account.

In the present study, off-axis compressive strength and its strain-rate dependence in a quasi-static range are studied for a unidirectional carbon/epoxy laminate at a high temperature. Also tested are the Tsai-Wu failure criterion and a physically based criterion for accuracy of prediction

of off-axis compressive strength at different strain rates at high temperature. By comparing the off-axis compressive test data with the results from off-axis tension tests, an asymmetry of strength in tension and compression at high temperature is elucidated for different strain rates. Finally, an extended formulation of a viscoplasticity model for unidirectional composites considering the tension-compression asymmetry in nonlinear deformation preceding ultimate failure is attempted. Validity of the modified viscoplasticity model is evaluated on the basis of comparisons between predicted and observed stress-strain behaviors upon off-axis tensile and compressive loading at different strain rates.

2. Material and Experimental Procedure

2.1 Material and specimen

The material used in this study is a unidirectional carbon/epoxy laminate fabricated from the prepreg tape T800H/2500 (TORAY). The lay-up of virgin laminates is $[0]_{12}$, and they were cured at 130°C in an autoclave. The thickness of as-cured laminates was 2.2 mm.

Six kinds of plain coupon specimens with different fiber orientations (θ = 0, 10, 15, 30, 45, 90°) were cut from 400 mm by 400 mm unidirectional laminate panels. For static tension tests, long specimens based on the testing standards JIS K 7073, ASTM D3039, JIS K 7083 and ASTM D3479 were employed; the dimensions were length L = 200 mm, gauge length L_G = 100 mm and width W = 20 mm. For static compression tests, on the other hand, short specimens were used to reduce the risk of buckling of specimen; the dimensions were length L = 100 mm, gauge length L_G = 10 mm, and width W = 10 mm.

2.2 Testing procedure

Off-axis monotonic tension and compression tests were performed at 100°C under stroke control. Two different constant values of displacement rate, 1.0 and 0.01 mm/min, were chosen for each fiber orientation. These static tests were conducted in a closed-loop hydraulic MTS-810 testing machine. For raising the temperature of specimens, a heating chamber with a precise digital control capability was employed. Anti-bucking guides were not used.

3. Experimental Results and Discussion

3.1 Comparison between off-axis tensile and compressive stress-strain curves

Figs. 1 (a), (b) show comparisons of the off-axis compressive stress-strain curve with that obtained from off-axis tension test under the same condition (1.0 mm/min, 100°C) for the off-axis fiber orientations θ = 10, 45°, respectively. The compressive stress-strain curves for the specimens fractured in a typical compressive failure mode are plotted on these figures. In these figures, it is clearly seen that the off-axis compressive stress-strain curve has a higher stress level than the off-axis tensile stress-strain curve, regardless the fiber orientation. This reveals that the flow stress required for continuing off-axis nonlinear compressive deformation is much larger than that for continuing off-axis nonlinear tensile deformation.

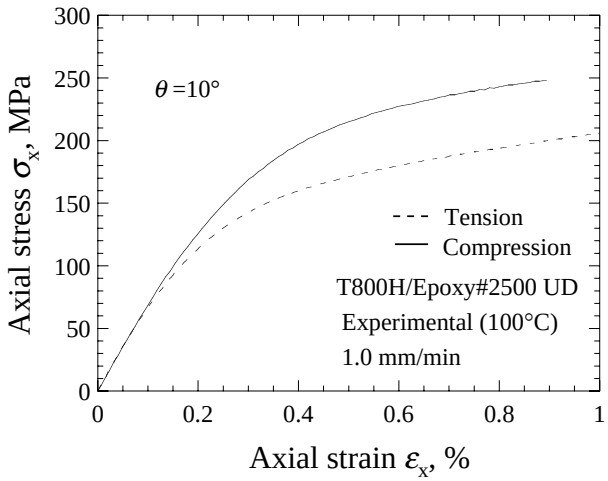

(a) θ = 10°

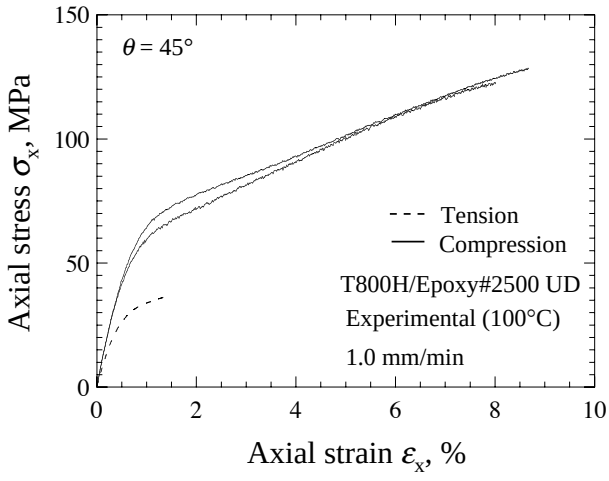

(b) θ = 45°

Fig. 1 Comparison of off-axis tensile and compressive stress-strain curves

The same off-axis compression tests were performed using two specimens for all fiber orientations. The stress-strain relationships obtained from the two compression tests agreed well with each other with great accuracy for the fiber orientations θ = 45, 90°. However, for small off-axis angles (θ = 10, 15°), the compressive flow stress significantly varied depending on the dominant failure mode, which is discussed later on.

The off-axis compressive stress-strain curves for the specimens failed in an in-plane shear mode agreed well with those obtained from tension tests, unlike the compressive stress-strain curves shown in Fig. 1 for the specimens fractured in an out of plane shear mode (i.e. transverse compressive failure). The reason for occurrence of either tensile or compressive failure mode for the fiber orientations θ = 10, 15° may be interpreted as follows: 1) the in-plane shear stress along then fibers is relatively high; 2) the in-plane shear failure is caused by a relatively lower stress; 3) the in-plane shear failure along the fibers is constrained by the end tabs in short specimens, inducing the out-of-plane shear failure instead.

3.2 Off-axis compressive strength

The off-axis compressive strengths obtained from compression tests at a constant strain rate of 1.0 mm/min are plotted in Fig. 2 as a function of fiber orientation angle. Two data obtained for each fiber orientation are indicated by different symbols; the open circles ○ represent higher strength data, and the filled circles ● represent lower strength data. The dotted line indicates the level of off-axis tensile strength predicted using the Tsai-Hill static failure criterion for the same strain rate and test temperature (1 mm/min, 100°C); it has been confirmed that the Tsai-Hill predictions agree well with experimental results, although those data points are omitted to highlight the compressive data points.

The off-axis compressive strengths for the fiber orientations θ = 30, 45, 90° are 2.1, 3.3, and 3.2 times larger than the off-axis tensile strengths for the same fiber orientations, respectively. The off-axis compressive strengths of two specimens with the same fiber orientations θ = 30, 45, 90° agree well with each other.

By contrast, a significant fluctuation was observed in the off-axis compressive strengths measured for θ = 10, 15°. From this figure, it is seen that the lower values of those compressive strength data (●) fall onto the dotted line representing the

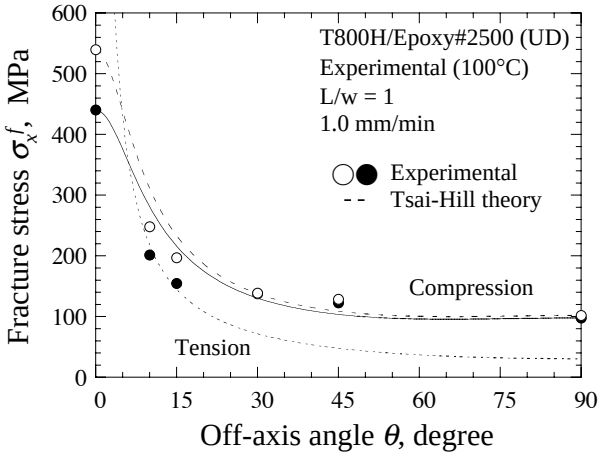

Fig. 2 Fiber orientation dependence of off-axis compressive strength at 1.0 mm/min

predicted tensile strengths. Those compressive strength data came from the specimens that failed predominantly by the in-plane shear failure mode similar to the tensile failure mode in the same range of off-axis fiber orientation. This explains the reason for good agreement of those lower compressive strength levels with the tensile strengths and appearance of the lower values in the off-axis compressive strengths for the small off-axis angles.

On the other hand, the higher values of the compressive strength data for θ = 10, 15° are obviously larger than the tensile strength indicated by the dotted line, and they almost fall onto the solid line in the figure which was obtained by fitting the Tsai-Hill failure criterion to the compressive strength data for θ = 30, 45, 90°. This implies that the higher values of the compressive strengths for θ = 10, 15° came from the specimens that was fractured in a compressive failure mode.

3.3 Off-axis compressive failure mode

The macroscopic failure modes of specimens fractured in static compression at the constant strain rate of 1.0 mm/min are shown in Fig. 3 for off-axis fiber orientations.

A splitting induced compressive failure was dominant in the fiber direction (θ = 0°), as shown in Fig. 3(a). For the fiber orientations θ = 10, 15°, specimens were fractured in either an in-plane shear failure mode or a combined kink-like and out-of-plane shear failure mode were observed; those two kinds of failure modes for θ = 10, 15° are shown in Figs. 3(b), (b') and Figs. 3(c), (c'), respectively. The compressive strength controlled by the combined kink-like and out-of-plane shear failure was larger

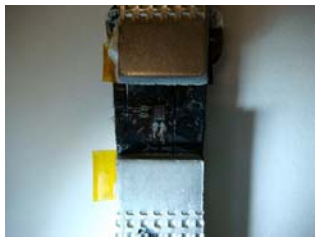

(a) $\theta = 0°$

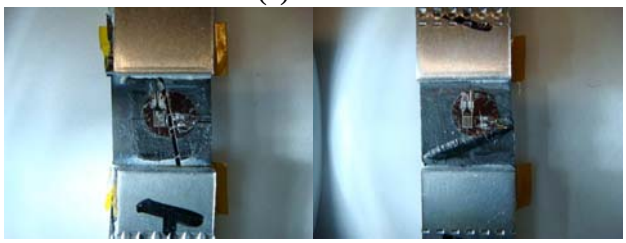

(b) $\theta = 10°$ (b') $\theta = 10°$

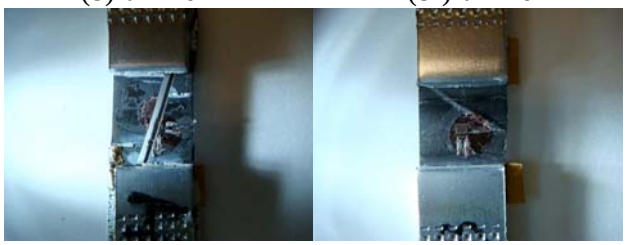

(c) $\theta = 15°$ (c') $\theta = 15°$

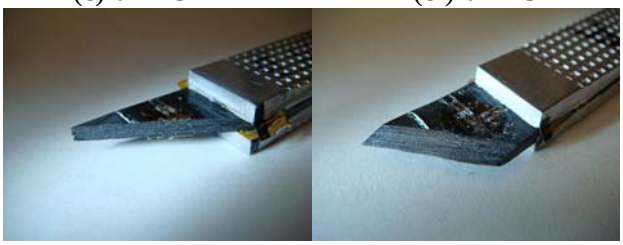

(d) $\theta = 30°$ (e) $\theta = 45°$

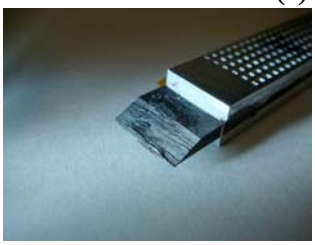

(f) $\theta = 90°$

Fig. 3 Failure morphology in off-axis compression at 1.0 mm/min

than that controlled by the in-plane shear failure. In the case of in-plane shear failure, the through-the-thickness fracture surface was almost perpendicular to the plane of load-fiber axes. This fiber/matrix interface controlled fracture mode in compression is similar to that observed in tension, which partly explains the reason for good agreement of the resulting compressive strength with the tensile strength and for the lower compressive strengths of

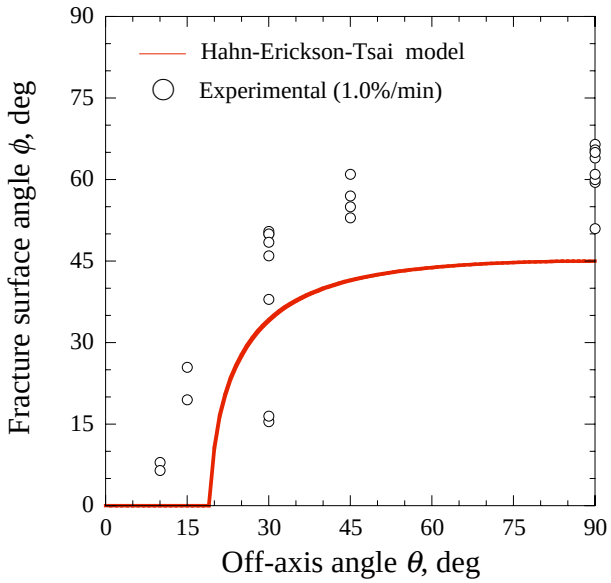

Fig. 4 Angle of fracture plane with through-the-thickness direction under off-axis compression at 1.0 mm/min

the specimens fractured in this failure mode. Figs. 3(d), (e), (f) show the macroscopic compressive failure modes for $\theta = 30$, 45 and 90°, respectively. It is clearly observed that the fracture surface is parallel with the fibers and it is appreciably inclined from the through-the-thickness direction of the specimens.

The angle of the fracture surface with the through-the-thickness direction increases from 0 to 65° with the increase in off-axis angle θ. The angle of fracture surface with the through-the-thickness direction is shown in Fig. 4 as a function of off-axis fiber orientation. This reveals that these specimens failed along the fibers in a combined in-plane and out-of-plane matrix shear mode. The area of failure surface increases with the inclination of the failure surface, suggesting larger energy consumption with failure. This partly explains the reason for the increase in off-axis compressive strength compared with tensile strength as the off-axis angle increases.

Consequently, it is considered that the gradual change in failure mode with increasing θ from the in-plane shear fracture to the combined in-plane and out-of-plane shear fracture results in the larger off-axis compressive strengths.

3.4 Rate dependence of off-axis compressive strength

Fig. 5 shows comparisons the off-axis compressive strengths measured at the two strain rates of 1.0 and

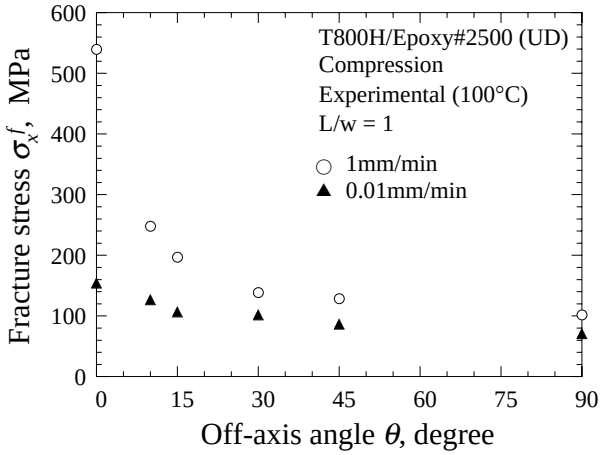

Fig. 5 Comparison of off-axis compressive strengths at different strain rates

0.01 mm/min. It is seen that the off-axis compressive strength at the lower strain rate is smaller by 10 to 20% than that at the higher strain rate, except for the fiber direction. The observed strain-rate dependence of the off-axis compressive strength is comparable to that of the off-axis tensile strength at the same test temperature.

Comparison with the values calculated using the tension test results at the same strain rate shows that the longitudinal compressive strength reduces to 65% of the longitudinal tensile strength and the transverse and shear strengths increase by the factors of 3.4 and 1.5 respectively. A marked strain-rate dependence of the transverse and shear strength can clearly be observed. The ratios of the principal strengths from the compression test data at 0.01 mm/min to those from the tension test data are comparable to the results at 1.0 mm/min.

4. Prediction of Off-Axis Strength

4.1 Phenomenological failure criteria

The Tsai-Wu failure criterion and a physically based criterion are tested for accuracy of prediction of off-axis tensile and compressive strengths at different strain rates at high temperature.

A simple failure criterion, called an interfacial friction based failure criterion hereafter, which considers a friction stress on a sliding fracture surface as well as a tension-compression asymmetry in the longitudinal and transverse strengths is first formulated. The interfacial friction based failure criterion considered in this study consists of two different formulae based on the Tsai-Hill failure criterion:

$$\left(\frac{\sigma_{11}}{X_T}\right)^2 - \frac{\sigma_{11}\sigma_{22}}{{X_T}^2} + \left(\frac{\sigma_{22}}{Y_T}\right)^2 + \left(\frac{\sigma_{12}}{S}\right)^2 = 1 \qquad (1)$$

for off-axis tensile loading and

$$\left(\frac{\sigma_{11}}{X_C}\right)^2 - \frac{\sigma_{11}\sigma_{22}}{{X_C}^2} + \left(\frac{\sigma_{22}}{Y_C}\right)^2 + \left(\frac{\sigma_{12}}{S-\mu_L\sigma_{22}}\right)^2 = 1 \qquad (2)$$

for off-axis compressive loading. The friction stress on a sliding failure surface depends on both compressive normal stress and a coefficient μ_L. Note that elimination of the first and second terms in the right hand side of Eq. (2) leads to a simpler form of matrix dominated failure criterion.

4.2 Comparison with experimental results

4.2.1 Predictions using the Tsai-Wu criterion

Comparisons between the predictions using the Tsai-Wu failure criterion and the experimental data are first shown in Fig. 6 for the strain rate of 1.0 mm/min. The predicted tensile and compressive strengths agree well with the experimental results over the range of off-axis angle, regardless of the strain rate.

Fig. 7 shows the failure envelope predicted using the Tsai-Wu failure criterion for the strain rate of 1.0 mm/min, together with symbols representing the experimental data. Significant disagreement is found between the predicted and experimental failure envelopes in the $\sigma_{22}\tau_{12}$-plane, especially in the second quadrant, in contrast to the good agreement between the predicted and experimental failure stresses shown in Fig. 6. Obviously, the inaccuracy of prediction regarding the level of resolved shear stress is more appreciable at a higher compressive normal stress, which corresponds to the compressive failure in the range of fiber orientation $30 \le \theta < 90°$. This observation suggests the need for a more improved criterion for shear failure.

4.2.2 Predictions using the interfacial friction based failure criterion

The fiber orientation dependence of the off-axis tensile and compressive strengths predicted using the interfacial friction based failure criterion is shown in Fig. 8 for the strain rate of 1.0 mm/min, and the associated failure envelope in the $\sigma_{22}\tau_{12}$-plane is presented in Fig. 9. In these calculations, the shear strengths evaluated using the tension test data

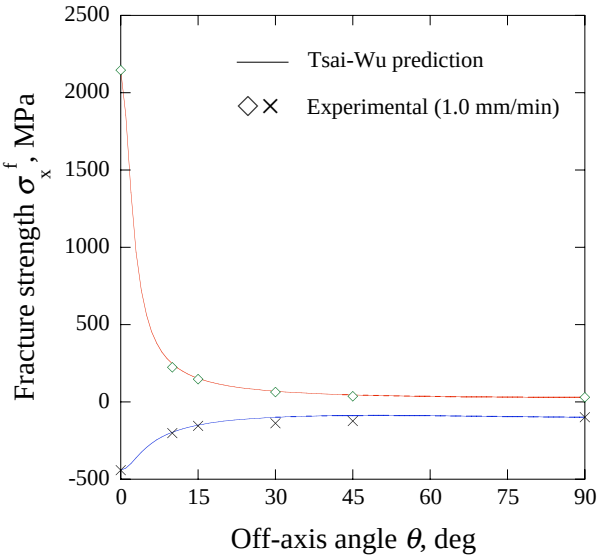

Fig. 6 Off-axis compressive strength predicted using the Tsai-Wu failure criterion (1.0 mm/min)

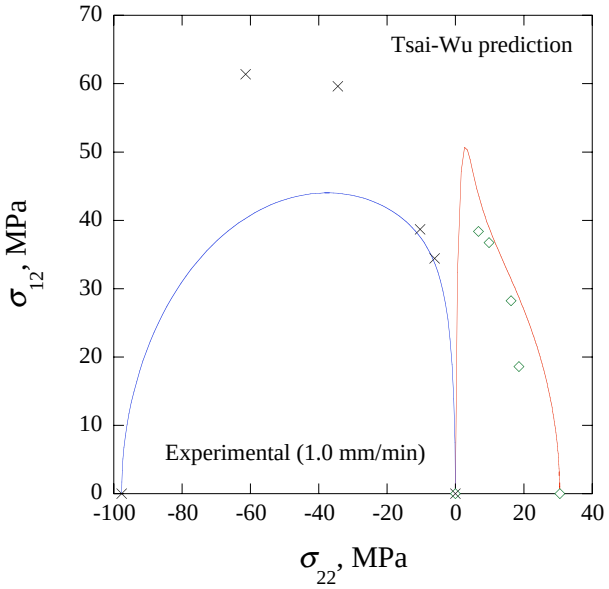

Fig. 7 Failure envelope for off-axis tension and compression and predictions using the Tsai-Wu failure criterion (1.0 mm/min)

for respective strain rates were assumed, and a constant value of 0.8 was used for the coefficient of friction.

Fig. 8 demonstrates that the off-axis tensile and compressive strengths and their fiber orientation dependence are accurately predicted using the interfacial friction based failure criterion. A little more detailed observation helps us to notice that the shape of the compressive strength versus off-axis angle curve predicted using the interfacial friction based failure criterion has inflection points at off-axis angles around θ = 40°. It appears that this intrinsic feature has contributed the excellent agreement with the experimental data. Note that the curve predicted using the Tsai-Wu failure criterion is concave over the range of fiber orientation.

The failure envelope is successfully predicted using the interfacial friction based failure criterion as well, regardless of the strain rate, as clearly observed in Fig. 9. It is obvious that the accuracy of prediction

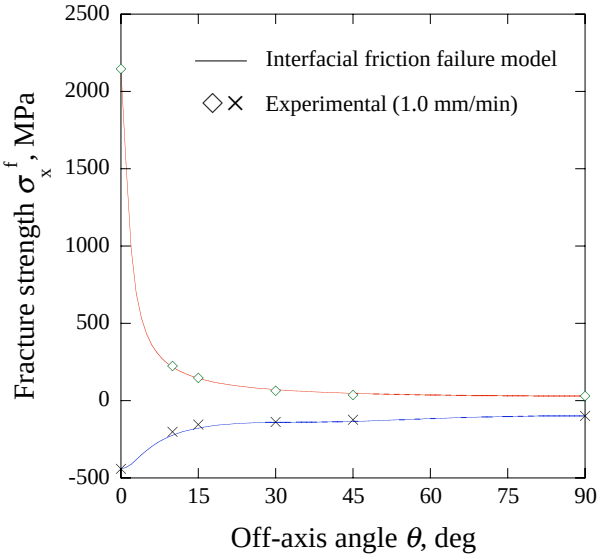

Fig. 8 Off-axis compressive strength predicted using the friction-based failure criterion (1.0 mm/min)

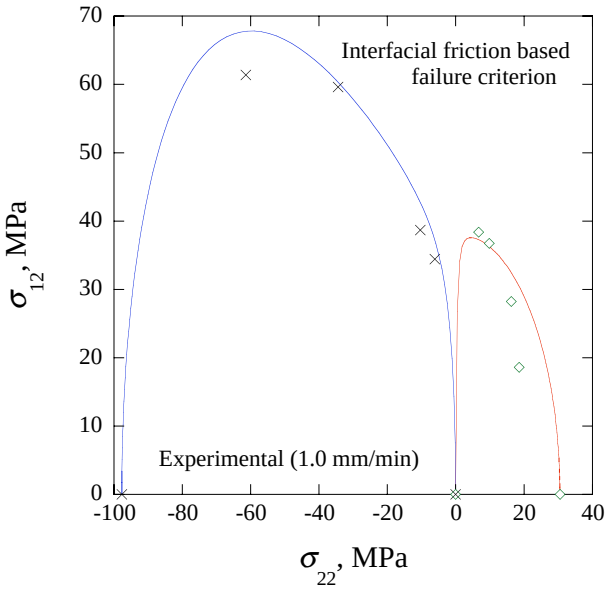

Fig. 9 Failure envelope for off-axis tension and compression and predictions using the friction-based failure criterion (1.0 mm/min)

of failure envelope in the $\sigma_{22}\tau_{12}$ –plane is much improved, compared with the prediction using the Tsai-Wu failure criterion. This observation strongly supports that the effect of shear stress sign on shear strength can effectively be considered by incorporating a friction stress on the fracture surface into a failure criterion.

4.3 Out-of-plane shear failure surface

The angle of the fracture surface with the through-the-thickness direction of coupon specimens can approximately be calculated using the Hahn-Erickson-Tsai model [7]. The failure surface angles measured using the photographs of specimens fractured under off-axis compressive loading are plotted in Fig. 4 as a function of off-axis angle. The failure surface begins to incline at an off-axis angle in the range θ = 10 ~ 20° after incubation, and increases up to a value of 65°. The angle of the failure surface for the transverse compression (θ = 90°) is greater than 45°. The reason why the inclination is greater than 45° may be due to the friction stress acting on the failure surface. This observation suggests that the effect of friction on shear strength should appropriately be considered in the analysis of ultimate fracture strength. Also, this observation indirectly supports the validity of the interfacial friction based failure criterion examined above.

5. A Viscoplasticity Model Considering Tension-Compression Asymmetry

In the present study, a simple extension to the effective stress and effective plastic strain proposed by Sun and Chen [8] is made to describe the different nonlinear deformation behavior in tension and compression without yielding any inelastic strain in the fiber direction. By means of the extended effective stress and effective viscoplastic strain rate, the viscoplasticity model with isotropic hardening [9, 10] is generalized which is furnished with an enhanced capability to describe the asymmetric off-axis nonlinear viscoplastic deformation behavior of the off-axis viscoplastic deformation of unidirectional composites. The proposed viscoplasticity model is tested for predictive accuracy by comparing the predicted and experimental results.

A plane stress formulation is considered. Stress and viscoplastic strain rate vectors are then defined as

$$\boldsymbol{\sigma} = \{\sigma_{11}, \sigma_{22}, \tau_{12}\}^T \tag{3}$$

$$\dot{\boldsymbol{\varepsilon}}^p = \{\dot{\varepsilon}_{11}^p, \dot{\varepsilon}_{22}^p, \dot{\gamma}_{12}^p\}^T \tag{4}$$

where vector components are taken with respect to the principal material coordinate system.

5.1 Effective stress and effective viscoplastic strain rate

The equivalent stress is modified as

$$\bar{\sigma} = \sqrt{\frac{3}{2}\boldsymbol{\sigma}\cdot\mathbf{B}\boldsymbol{\sigma}} \tag{5}$$

where,

$$\mathbf{B} = \begin{bmatrix} 0 & 0 & 0 \\ 0 & b_{22} & 0 \\ 0 & 0 & b_{66} \end{bmatrix} \tag{6}$$

$$b_{22} = \beta \tag{7}$$

$$b_{66} = 2a_{66}\beta \tag{8}$$

$$\beta = (1-\alpha)H(\sigma_{22}) + \alpha \tag{9}$$

The function H involved by the above equation is the Heaviside function defined as

$$H(x) = \begin{cases} 1 & x \geq 0 \\ 0 & x < 0 \end{cases} \tag{10}$$

Considering that the effective stress and effective plastic strain increment should be energy conjugate with each other, we can derive the following modified expression of the effective strain rate:

$$\bar{\dot{\varepsilon}}^p = \sqrt{\frac{2}{3}\left[\frac{1}{b_{22}}(\dot{\varepsilon}_{22}^p)^2 + \frac{1}{b_{66}}(\dot{\gamma}_{12}^p)^2\right]} \tag{11}$$

5.2 An extended viscoplasticity model

In phenomenological viscoplasticity models for engineering materials, a master relationship between the effective viscoplastic strain rate $\bar{\dot{\varepsilon}}^p$ and an

effective oversress $\bar{H}$ is assumed, and it is typically expressed in the form

$$\dot{\bar{\varepsilon}}^p = \left\langle \frac{\bar{H}}{K} \right\rangle^{\frac{1}{m}} \tag{12}$$

where K and m are material constants. The angular brackets in equation (1) denote the operation: $< x >$ = x ($x \geq 0$); $< x >$ = 0 ($x < 0$). The effective overstress $\bar{H}$ represents the magnitude of a net stress that determines the magnitude of the viscoplastic strain rate.

By using the extended effective stress $\bar{\sigma}$ given by Eq. (5), a simple form of the effective overstress is defined as

$$\bar{H} = \bar{\sigma} - r - \sigma_0 \tag{13}$$

where r is a scalar hardening variable to describe the time- and rate-dependent behavior. The parameter σ_0 characterizes an initial elastic response, and it may be treated as an initial value of r. Then, the viscoplastic strain rate can be expressed as

$$\dot{\boldsymbol{\varepsilon}}^p = \left\langle \frac{\bar{\sigma} - r - \sigma_0}{K} \right\rangle^{\frac{1}{m}} \frac{3}{2} \mathbf{B}\boldsymbol{\sigma} \tag{14}$$

The viscoplasticity model is characterized by the evolution equation of the isotropic hardening variable r. In the present study, we assume the following expression:

$$\dot{r} = \sum_a b^{(a)} \left(Q^{(a)} - r^{(a)} \right) \dot{\bar{\varepsilon}}^p \tag{15}$$

where Q_i stands for the saturated value of r_i, and a material constant b_i characterizes the manner in which r_i approaches the saturated value. The multi-component representation of the evolution equation of r, Eq. (15), in the viscoplasticity model provides excellent flexibility in describing the nonlinear response of individual plies. Normally, two or three components are taken to describe the nonlinear stress-strain behavior under simple loading conditions.

5.3 Comparison of predicted and experimental results

All parameters except for newly introduced α can be determined in the same manner as in the Gates-Sun model. The detail of the procedure for material identification can be seen in the previous reports [9, 10]. The parameter α is determined in such a way that the master relationship for $\theta = 90°$ in tension agrees well with that in compression.

Comparisons of the predicted and observed off-axis stress-strain curves at the strain rate of 1.0 mm/min are shown in Fig. 10 for both tension and

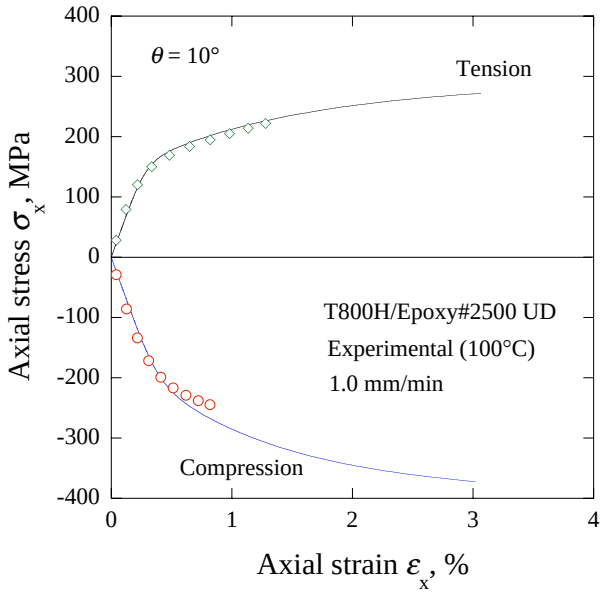

(a) $\theta = 10°$

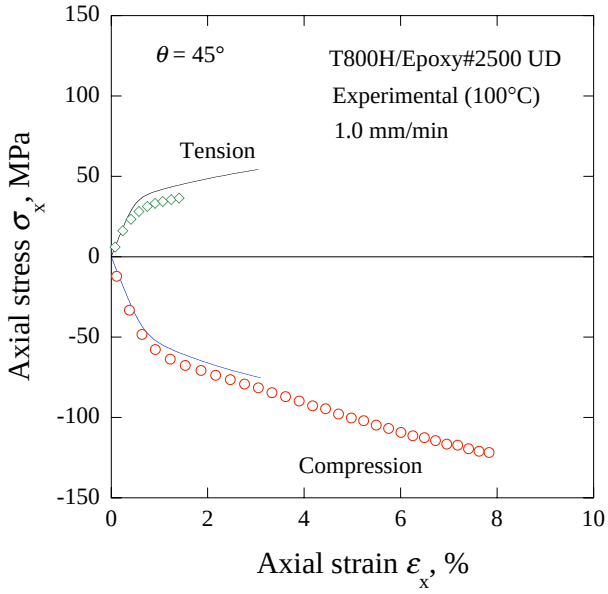

(b) $\theta = 45°$

Fig. 10 Predicted off-axis tensile and compressive stress-strain curves (1.0 mm/min)

and compression. Deviation of the predicted results from the experimental results can be found. Nevertheless, overall, the different behaviors in tension and compression, fiber orientation dependence of off-axis stress-strain curve and strain rate dependence have been described with favorable accuracy. Note that these results have been predicted using a single constitutive model. Consequently, it is considered that promising agreements have been achieved.

6. Conclusion

(1) The off-axis compressive strengths for the fiber orientations θ = 30, 45, 90° are about 2 ~ 3 times larger than the off-axis tensile strengths.
(2) The magnitude of off-axis compressive strength significantly depends on the rate of loading, and the off-axis compressive strength at a lower strain rate of 0.01%/min was 10 to 30% lower than the values measured at 1.0%/min.
(3) For the small off-axis angles θ = 10, 15°, the off-axis compressive strength varies according to the type of dominant failure mode. When the compressive failure occurs in an in-plane shear failure mode, a relatively low off-axis compressive strength is measured which almost agrees with the off-axis tensile strength of a specimen with the same fiber orientation. On the other hand, the compressive failure mode characterized by a combination of kink-like failure with a slight out-of-plane shear leads to a higher compressive strength, compared with the off-axis tensile strength.
(4) The off-axis compressive failure occurs in a combined in-plane and out-of-plane shear failure mode for the fiber orientations θ = 30, 45°, and predominantly in a out-of-plane shear failure mode for θ = 90°. The angle of the fracture surface with the through-the thickness direction increases from 0 to 65° with increasing off-axis angle.
(5) The fiber orientation dependence of the off-axis compressive strength can adequately be described using the Tsai-Wu failure criterion, regardless of the strain rate. Regarding the failure envelope in the stress plane spanned by the in-plane transverse stress and shear stress components, however, the prediction using the Tsai-Wu failure criterion significantly deviates from the experimental result.
(6) The Tsai-Hill failure criterion has been modified to include the effect of friction stress on shear failure. The resulting interfacial friction based failure criterion successfully describes not only the fiber orientation dependence of off-axis compressive strength, but also the failure envelope associated with the in-plane matrix/interface failure.
(7) The proposed viscoplasticity model succeeds in predicting the fiber orientation dependence of off-axis non-linear behavior, deformation asymmetry in off-axis tension and compression, and the strain rate dependence.

References

[1] Hahn HT. and Williams JG. “Compression failure mechanisms in unidirectional composites”. STP 893, ASTM, 1986.

[2] Berbinau P., Soutis C., Goutas P. and Curtis PT. “Effect of off-axis ply orientation on 0°-fibre microbuckling”. Composites part A, Vol. 30, pp 1197-1207, 1999.

[3] Kawai M. and Suda H. “Effects of non-negative mean stress on the off-axis fatigue behavior of unidirectional carbon/epoxy composites at room temperature”. Journal of Composite Materials, Vol. 38, No. 10, pp 833-854, 2004.

[4] Jones R.M. Mechanics of composite materials, Taylor and Francis, 2/E, 1999.

[5] Davila C.G., Camanho P.P. and Rose C.A. “Failure criteria for FRP laminates”. Journal of Composite Materials, Vol. 39, No. 4, pp 323-345, 2005.

[6] Pinho S.T., Iannucci L. and Robinson P. “Physically-based failure models and criteria for laminated fibre-reonforced composites with emphasis on fibre kinking: Part I: Development, Composites”. Vol. 37, pp 63-73, 2006.

[7] Hahn H.T., Erikson J.B. and Tsai S.W. “Characterization of matrix/interface-controlled strength of unidirectional composites”. Fracture of Composite Materials, Proceedings of the Second USA-USSR Symposium, Lehigh University, Bethlehem, Pennsylvania, USA, March 9-12, pp 197-214, 1981.

[8] Sun C.T. and Chen J.L. “A simple flow Rule for characterizing nonlinear behavior of fiber composites”. *Journal of Composite Materials*, Vol. 23, pp 1009-1020, 1989.

[9] Kawai M. and Masuko Y. “Macromechanical modeling and analysis of the viscoplastic behavior of unidirectional fiber-reinforced composites”. *Journal of Composite Materials*, Vol. 37, No. 21, pp 1885-1902, 2003.

[10] Kawai M. and Masuko Y. “Creep behavior of unidirectional and angle-ply T800H/3631 laminates at high temperature and simulation using a phenomenological viscoplasticity model”. *Composites Science and Technology*, Vol. 64, No. 15, pp 2373-2384, 2004.